This document is the accepted manuscript version of the following article:
Stolz, S., Di Giovannantonio, M., Urgel, J. I., Sun, Q., Kinikar, A., Borin Barin, G., … Widmer, R. (2020). Reversible dehalogenation in on‐surface aryl‐aryl coupling. Angewandte Chemie International Edition.
https://doi.org/10.1002/anie.202005443

Reversible dehalogenation in on-surface aryl-aryl coupling

Samuel Stolz,[1,2,†] Marco Di Giovannantonio,[1,†,*] José I. Urgel,[1] Qiang Sun,[1] Amogh Kinikar,[1] Gabriela Borin Barin,[1] Max Bommert,[1] Roman Fasel,[1,3,*] and Roland Widmer[1,*]

[1]*Empa, Swiss Federal Laboratories for Materials Science and Technology, nanotech@surfaces Laboratory, 8600 Dübendorf, Switzerland*
[2]*Institute of Physics, École Polytechnique Fédérale de Lausanne, Laboratory of Nanostructures at Surfaces, CH-1015 Lausanne, Switzerland*
[3]*Department of Chemistry and Biochemistry, University of Bern, 3012 Bern, Switzerland*
[†]*These authors contributed equally*

In the emerging field of on-surface synthesis, dehalogenative aryl-aryl coupling is unarguably the most prominent tool for the fabrication of covalently bonded carbon-based nanomaterials. Despite its importance, the reaction kinetics are still poorly understood. Here we present a comprehensive temperature-programmed x-ray photoelectron spectroscopy investigation of reaction kinetics and energetics in the prototypical on-surface dehalogenative polymerization of 4,4''-dibromo-*p*-terphenyl into poly(*para*-phenylene) on two coinage metal surfaces, Cu(111) and Au(111). We find clear evidence for reversible dehalogenation on Au(111), which is inhibited on Cu(111) owing to the formation of organometallic intermediates. The incorporation of reversible dehalogenation in the reaction rate equations leads to excellent agreement with experimental data and allows extracting the relevant energy barriers. Our findings deepen the mechanistic understanding and call for its reassessment for surface-confined aryl-aryl coupling on the most frequently used metal substrates.

Keywords: aryl-aryl coupling, dehalogenation, reaction mechanisms, reversibility, surface chemistry.

Confining reactants onto a two-dimensional metallic surface is a powerful strategy for the synthesis of carbon-based nanomaterials that are elusive via wet chemistry.[1] In this context, thermally activated dehalogenative aryl-aryl coupling[2] has emerged as the most controllable and versatile on-surface reaction to covalently connect aryl halides under ultrahigh vacuum (UHV) conditions. Despite its extensive application to the on-surface synthesis of carbon nanostructures,[3–9] details of its reaction pathway are still lacking a comprehensive description.
The assessment of reaction pathways and products is usually performed employing scanning tunneling microscopy (STM) in combination with x-ray photoelectron spectroscopy (XPS), but neither of these techniques provide detailed time and temperature resolution of a dynamically evolving process. In this respect, temperature-programmed XPS (TP-XPS) is a unique tool to discern fundamental mechanistic aspects of thermally activated surface reactions that has also been applied to study dehalogenative aryl-aryl coupling reactions.[10–18] Such investigations have shown that the chemical transformations reflected in the halogen XPS signal are identical for many substrates, starting with the halogen's dissociation from the molecular precursor, accompanied by its chemisorption to the substrate, and its eventual desorption from the surface. Setting aside differences in the onset temperatures of these processes for different substrates and precursors, clear dissimilarities in the temperature evolution of the dehalogenation step are noted, i.e. more rapid *versus* gradual temperature progressions with a temperature interval ranging from about 30 to 100 K.[10,12,13,16,18] These different behaviors have been attributed to two

alternative reaction pathways: (i) the rapid formation of stable organometallic (OM) intermediates, and (ii) the radical stabilization by the substrate, followed by (more or less fast) covalent coupling.[18]

Here, we aim at unravelling the causes for such dissimilar dehalogenation dynamics and present a comparative study of 4,4''-dibromo-*p*-terphenyl (DBTP) as a model molecule undergoing dehalogenative homocoupling on Au(111) and Cu(111) surfaces (Figure 1).[19,20] The surface-assisted dehalogenative polymerization into poly(*para*-phenylene) (PPP) (Figure 1b,e) has been investigated by STM and TP-XPS. Our STM results reveal an average PPP length of 4.8 nm and 11.5 nm on Cu(111) and Au(111) respectively, as presented in Figure S1. We have designed an *ad hoc* experiment involving co-adsorbed chlorine atoms, which provides strong experimental evidence that debrominated DBTP radicals can be chlorinated on Au(111), thus implying a reversible dehalogenation mechanism on gold (Figure 1f). In contrast, such reversibility is not observed on Cu(111), where stable OM intermediates dominate after debromination (Figure 1c). Our results not only furnish a fundamental mechanistic insight into surface-confined aryl-aryl coupling but also set the basis for fine-tuning the dynamics of the product formation.

To study the dynamics of debromination in aryl-aryl coupling we have acquired TP-XPS maps (Figure 2) of a sub-monolayer coverage of DBTP deposited onto Au(111) and Cu(111) surfaces held at 300 K and 23 K (to avoid premature debromination), respectively. Each horizontal line of the maps shown in Figures 2a,d represents a single Br 3d core level doublet (Br $3d_{5/2}$ and Br $3d_{3/2}$) recorded during the 0.1 K/s heating ramp. With increasing temperature, a distinct chemical shift of the Br 3d doublet towards lower binding energy (BE) is observed. This chemical shift is due to debromination of the molecular precursor which occurs at different temperatures for Cu(111) (210 K) and Au(111) (350 K) according to their different catalytic activity. Polymerization and debromination happen simultaneously around 350 K on Au(111) (Figure S6b), whereas on Cu(111) the polymerization step is clearly distinct from the debromination one and occurs at 390 K (Figure S8), being preceded by the formation of a stable OM intermediate (Figure 1a). At high temperatures (above 600 K for Cu(111) and 550 K for Au(111)), a decrease in the overall Br 3d core level intensities is observed, which reflects bromine desorption from the surface. At the temperatures relevant for dehalogenation and polymerization, however, detached Br atoms remain adsorbed on both surfaces (Figure 1a,b,e), and we have not further studied Br desorption.

10.1002/anie.202005443

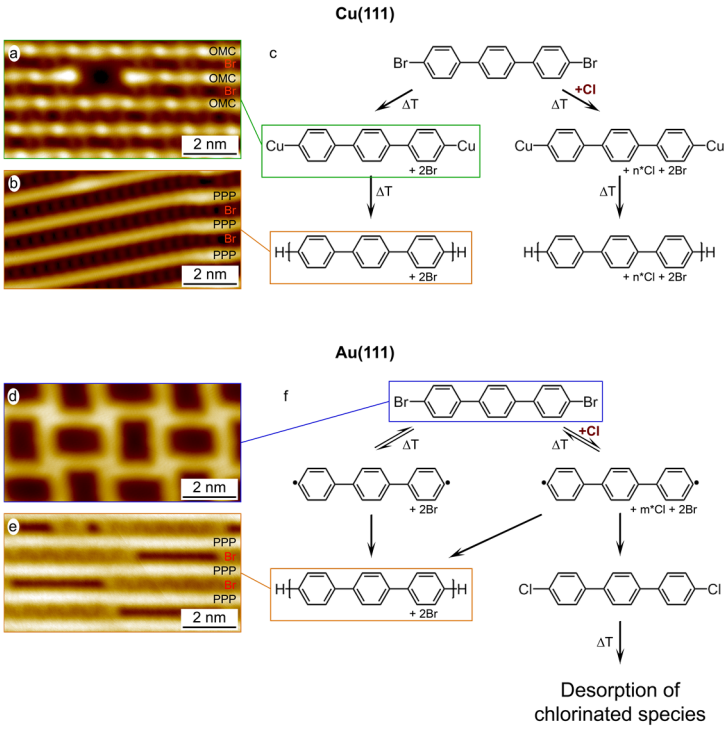

Figure 1 | Reaction mechanisms
STM images of DBTP after 300 K deposition on **a** Cu(111) (V_G = 0.05 V; I_T = 100 pA), forming OM chains and **d** Au(111) (V_G = 0.05 V; I_T = 200 pA), on which DBTP remains intact. PPP chains are obtained after annealing to 450 K on **b** Cu(111) (V_G = 0.1 V; I_T = 200 pA) and **e** Au(111) (V_G = -1.0 V; I_T = 200 pA) with Br atoms lying in-between. Reaction schemes of DBTP and DBTP co-adsorbed with Cl on **c** Cu(111) and **f** Au(111).

A striking difference between the two substrates is seen in the thermal evolution of DBTP debromination, highlighted by the kinetic curves extracted from the corresponding TP-XPS maps (Figure 2b,c). Debromination takes place between 200-230 K on Cu(111) and between 300-420 K on Au(111); thus over an approximately four times larger temperature interval in case of Au(111). If such "slower" debromination was due to radical molecules that, apart from homocoupling, could also recombine with Br atoms, it should be possible to passivate some of them by offering another reaction path. Therefore, we have co-deposited chlorine (which has a higher dissociation enthalpy than bromine[21]) with DBTP on Au(111) and Cu(111), with the aim of assessing whether chlorinated molecules could be detected during the heating ramp.

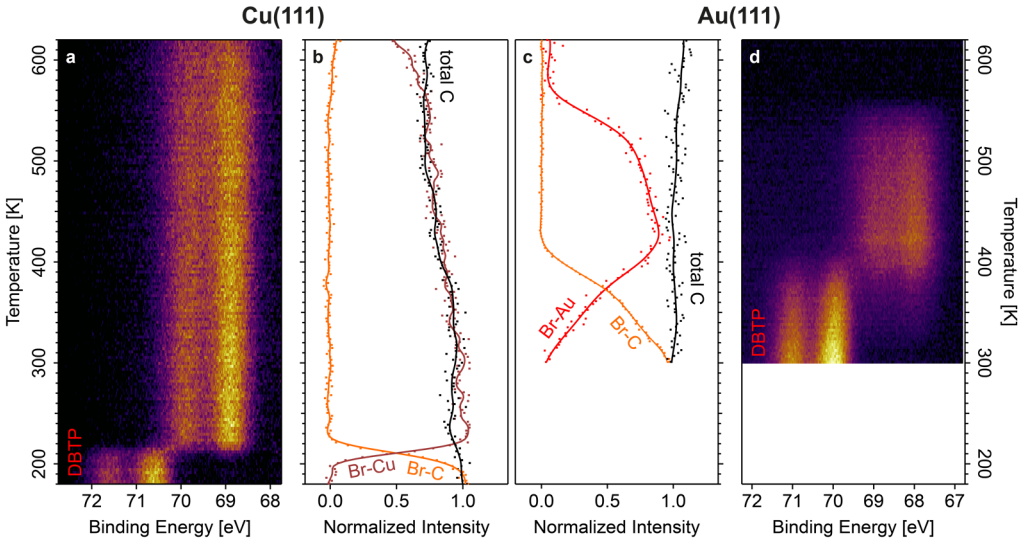

10.1002/anie.202005443

Figure 2 | Temperature evolution of DBTP on Cu(111) and Au(111)
TP-XPS maps of the Br 3d doublet during the annealing of DBTP on **a** Cu(111) and **d** Au(111). **b, c** Temperature dependence of the Br-C and Br-Metal signals extracted from these TP-XPS maps together with the total intensity of the C 1s signal, with the experimental data (dots) interpolated by a spline function (solid lines).

When chlorine is co-deposited with DBTP onto Cu(111) and the sample then annealed, no particular differences are observed in comparison to the standard growth of PPP from DBTP in absence of chlorine (Figure 3). In contrast, the growth of PPP on Au(111) presents distinct features in presence of co-deposited chlorine. In this case, the TP-XPS maps of simultaneously recorded Br 3d and Cl 2p (and C 1s) core levels in Figure 4a,b (and Figure S6c) reveal a clear chemical shift of the chlorine doublet (Cl $2p_{3/2}$ and Cl $2p_{1/2}$) to higher BE. As evidenced by the kinetic curves extracted from the Br 3d and Cl 2p TP-XPS maps (Figure 4c), the increase of the Cl-C and the simultaneous decrease of the Cl-Au component coincide with the bromine detachment from the molecules. This is also confirmed by high-resolution XPS spectra (Figure 4d, S6d) acquired at 300 K and 450 K: after complete DBTP debromination, the Br $3d_{5/2}$ core level is shifted from 69.3 eV to 67.8 eV, while Cl $2p_{3/2}$ is partially shifted from 197.0 eV to 199.3 eV and the C 1s halogen component from 284.5 eV to 284.8 eV. After reaching a maximum at 450 K, the Cl-C intensity is reduced, concurrently with the total carbon amount, indicating desorption of chlorinated molecules from Au(111) to be more favorable than dechlorination (Figure 4c, S7). All these observations clearly demonstrate that the radicals created at the carbon atoms upon debromination can again be attacked by halogens present on the surface. This provides unprecedented experimental evidence of reversible on-surface dehalogenation.

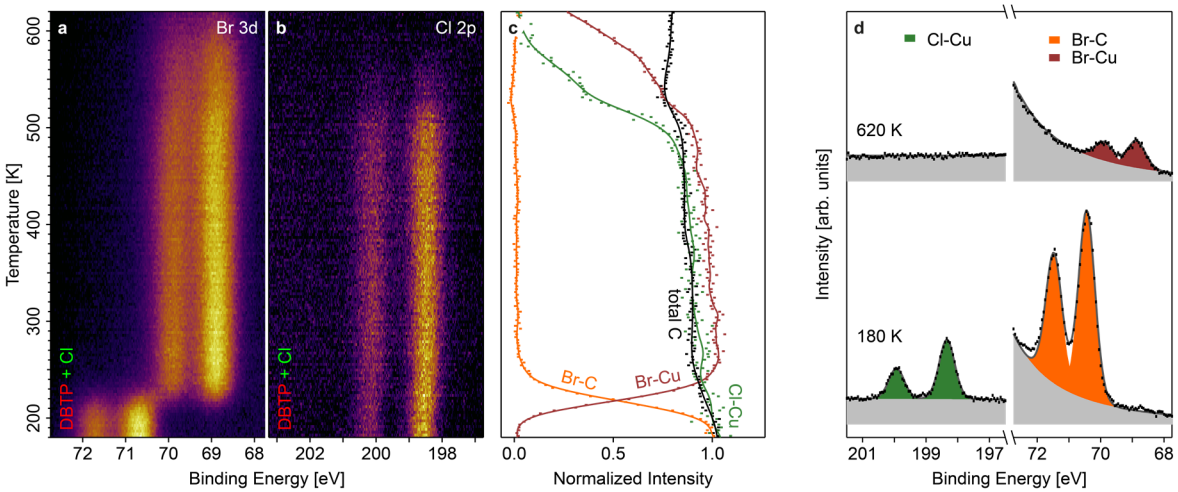

Figure 3 | Temperature evolution of DBTP + Cl on Cu(111)
TP-XPS maps of **a** Br 3d and **b** Cl 2p doublets during the annealing of DBTP + Cl on Cu(111). **c** Temperature dependence for all chemical states of Cl and Br, together with the total carbon coverage. The trend of each experimental curve (dots) is indicated with a spline (solid line). **d** High-resolution XPS for DBTP + Cl on Cu(111). Cl 2p (left) and Br 3d (right) doublets of the as prepared sample (bottom) and after almost complete halogen desorption (top).

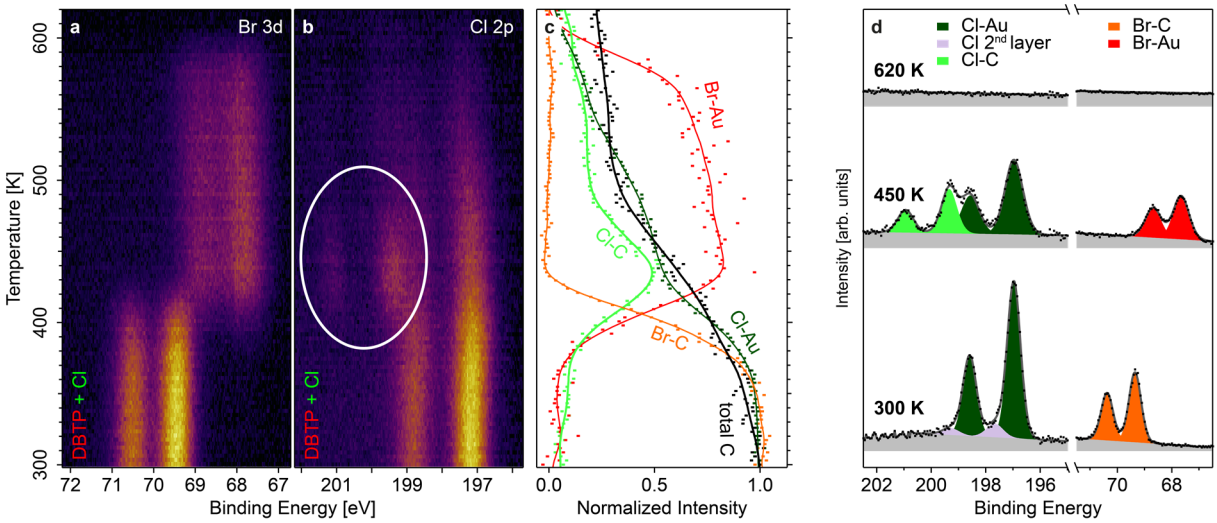

Figure 4 | Temperature evolution of DBTP + Cl on Au(111): Halogen exchange
TP-XPS maps of **a** Br 3d and **b** Cl 2p doublets during the annealing of DBTP + Cl on Au(111). The emergence of the Cl-C component is indicated with a white circle in **b**. **c** Temperature dependence for all chemical states of Cl and Br, together with the total carbon coverage. The trend of each experimental curve (dots) is indicated with a spline (solid line). **d** High-resolution XPS for DBTP + Cl on Au(111). Cl 2p (left) and Br 3d (right) doublets of the as prepared sample (bottom), after halogen exchange (center) and after halogen desorption (top).

Prompted by these findings, we included this so far neglected reversibility in the differential rate equations used to fit the experimental kinetic curves (*vide infra*). The relevant experimental kinetic curves extracted from the TP-XPS maps, i.e. the Br-C and Br-Metal components for Cu(111) and additionally the C-C component for Au(111), are reported in Figure 5. The dehalogenative aryl-aryl coupling on both surfaces can be described by the following reaction pathway

$$A \underset{k_{-1}}{\overset{k_1}{\rightleftarrows}} B + X$$
$$2B \xrightarrow{k_2} C$$

where A, B, X and C represent the intact DBTP precursor, the intermediate (OM on Cu(111), molecular radicals on Au(111)), the chemisorbed bromine atom and the covalently coupled product (i.e. PPP), respectively. k_1, k_{-1} and k_2 are the kinetic constants for each reaction step, i.e. DBTP debromination, re-bromination of intermediate, and C-C coupling.
Owing to the high energetic stability of the OM on Cu(111), the re-bromination process is suppressed on this surface. Consequently, the rate equations describing DBTP debromination (polymerization) reduce to a first (second) order Polanyi Wigner equation,[22] well reproducing the corresponding experimental kinetic curves (Figure 5a, S8).
In case of Au(111) the experimental kinetic curves cannot be successfully fit with a Polanyi-Wigner equation (Figure S9), instead we need the whole set of differential rate equations including reversibility of the dehalogenation (Figure 5a, see Supporting Information for further details). Our excellent fit confirms that the extended temperature range for debromination observed on Au(111) is associated to reversibility of this process, competing with the irreversible C-C bond formation, i.e. polymerization.
Moreover, the fits performed in the two cases provide the activation energies for the involved processes (Figure 5b). Debromination of DBTP on Cu(111) requires 0.62 eV and the conversion of the OM assembly into polymers 1.08 eV to be initiated. In contrast, on Au(111) the energy barrier for debromination, 0.95 eV, is larger than the one on Cu(111) and the created molecular radicals are energetically unfavorable and hence immediately subject to two possible pathways (Figure 1): (i) back reaction towards the formation of intact DBTP (0.67 eV), or (ii) covalent coupling towards the formation of PPP chains (0.70 eV).

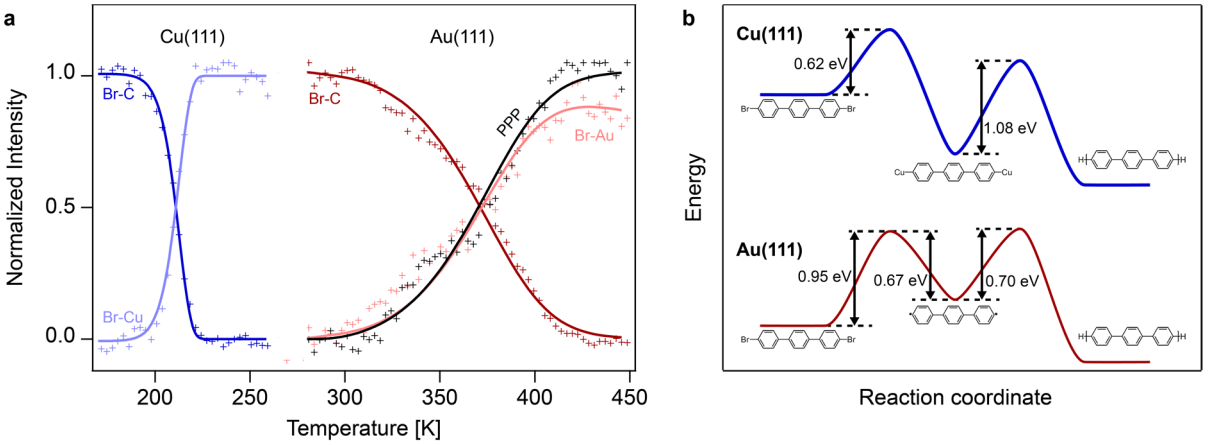

Figure 5 | Kinetic model
a Temperature evolution of Br-C, Br-Metal and PPP normalized signals extracted from the TP-XPS maps (markers) and fitted with the kinetic models for Cu(111) and Au(111) described in the text (solid lines). **b** Experimentally derived reaction profiles for the PPP formation from DBTP on the two substrates. The energy barriers have been obtained from fitting the kinetic curves in **a** and Figure S8.

Our experimentally determined energy barriers are in good agreement with those estimated using density functional theory (DFT).[18,23] In particular, for bromobenzene on Cu(111) Björk *et al.*[23] reported a bromine dissociation barrier of 0.66 eV yielding a surface bound radical that is about 0.7 eV more stable than the precursor, which suppresses re-bromination in accordance with our experimental results. On the other hand, the debromination barrier for bromobenzene on Au(111) is roughly 1 eV, resulting in a phenyl radical which is energetically about as stable as the precursor itself. Debrominated 1,3,5-tris(4-bromophenyl)benzene (TBB) was even found to be 0.25 eV less stable than the brominated TBB on Au(111).[18] Both simulations of the debromination process on Au(111) thus indicate re-bromination to be energetically possible, in agreement with our observation. The energy barrier for the covalent coupling towards PPP chains on Au(111) mainly arises from the diffusion energy barrier of debrominated DBTP. Our experimentally derived value of 0.70 eV for debrominated DBTP (which consists of 3 phenyl rings) is between the DFT-calculated diffusion barriers of debrominated bromobenzene (0.22 eV; 1 phenyl ring) and debrominated TBB (1.2 eV; 4 phenyl rings).
Such deeper insight into dehalogenative aryl-aryl coupling offers a better mechanistic understanding of this broadly exploited on-surface reaction and is a prerequisite for improving its efficiency and selectivity. In absence of stable OM formation the rate-limiting step for polymerization is the breaking of C-halogen bonds, whose temperature can be lowered with the choice of halogen functionalization, thus limiting undesired side reactions. On the other hand, the temperature range of the dehalogenation process extends in case of reversibility, increasing the likelihood of cross-talk with potential additional reactions occurring at higher temperature.[7] Therefore, to optimize polymer length, the halogens would ideally detach from the precursor molecule at as low temperature as possible and desorb from the surface right after, while the resulting radicals would immediately undergo polymerization. From a different perspective, however, such conditions could be detrimental to the growth of extended crystalline two-dimensional networks, which benefit from reversibility in the covalent coupling step.[24–27] Therefore, depending on the type of on-surface reaction and conditions at which it takes place, it is crucial to select the best catalyst/reagents combination to achieve a specific desired product.

ASSOCIATED CONTENT

Supporting Information
The Supporting Information containing additional experimental results is available free of charge on the Wiley Publications website.

AUTHOR INFORMATION

Corresponding Authors
*E-mail: marco.digiovannantonio@empa.ch
*E-mail: roman.fasel@empa.ch
*E-mail: roland.widmer@empa.ch

Notes
The authors declare no competing financial interest

ACKNOWLEDGMENTS

This work was supported by the Swiss National Science Foundation under Grant No. 200020_182015 and No. 159690, the European Union's Horizon 2020 research and innovation program under grant agreement number 785219 (Graphene Flagship Core 2), and the Office of Naval Research (N00014-18-1-2708). Skillful technical assistance by Lukas Rotach is gratefully acknowledged. The XPS experiments were performed on the X03DA (PEARL) beamline at the Swiss Light Source, Paul Scherrer Institut, Villigen, Switzerland. We thank the beamline manager Matthias Muntwiler (PSI) for his support during the experiments, Alexandre Gobbo (PSI) for the implementation of the acquisition software to enable recording three energy levels simultaneously during TP-XPS experiments, and Shantanu Mishra for very fruitful discussions.

REFERENCES

[1] S. Clair, D. G. de Oteyza, *Chem. Rev.* **2019**, *119*, 4717–4776.

[2] M. Lackinger, *Chem. Commun.* **2017**, *53*, 7872–7885.

[3] L. Grill, M. Dyer, L. Lafferentz, M. Persson, M. V. Peters, S. Hecht, *Nat. Nanotechnol.* **2007**, *2*, 687–91.

[4] L. Lafferentz, V. Eberhardt, C. Dri, C. Africh, G. Comelli, F. Esch, S. Hecht, L. Grill, *Nat Chem* **2012**, *4*, 215–220.

[5] J. Cai, P. Ruffieux, R. Jaafar, M. Bieri, T. Braun, S. Blankenburg, M. Muoth, A. P. Seitsonen, M. Saleh, X. Feng, et al., *Nature* **2010**, *466*, 470–473.

[6] P. Ruffieux, S. Wang, B. Yang, C. Sánchez-Sánchez, J. Liu, T. Dienel, L. Talirz, P. Shinde, C. A. Pignedoli, D. Passerone, et al., *Nature* **2016**, *531*, 489–492.

[7] M. Di Giovannantonio, O. Deniz, J. I. Urgel, R. Widmer, T. Dienel, S. Stolz, C. Sánchez-Sánchez, M. Muntwiler, T. Dumslaff, R. Berger, et al., *ACS Nano* **2018**, *12*, 74–81.

[8] M. Di Giovannantonio, K. Eimre, A. V. Yakutovich, Q. Chen, S. Mishra, J. I. Urgel, C. A. Pignedoli, P. Ruffieux, K. Müllen, A. Narita, et al., *J. Am. Chem. Soc.* **2019**, *141*, 12346–12354.

[9] Y.-Q. Zhang, M. Paszkiewicz, P. Du, L. Zhang, T. Lin, Z. Chen, S. Klyatskaya, M. Ruben, A. P. Seitsonen, J. V. Barth, et al., *Nat. Chem.* **2018**, *10*, 296–304.

[10] M. Di Giovannantonio, M. El Garah, J. Lipton-Duffin, V. Meunier, L. Cardenas, Y. Fagot Revurat, A. Cossaro, A. Verdini, D. F. Perepichka, F. Rosei, et al., *ACS Nano* **2013**, *7*, 8190–8198.

[11] M. Di Giovannantonio, M. El Garah, J. Lipton-Duffin, V. Meunier, L. Cardenas, Y. Fagot-Revurat, A. Cossaro, A. Verdini, D. F. Perepichka, F. Rosei, et al., *ACS Nano* **2014**, *8*, 1969–1971.

[12] K. A. Simonov, N. A. Vinogradov, A. S. Vinogradov, A. V. Generalov, E. M. Zagrebina, N. Mårtensson, A. A. Cafolla, T. Carpy, J. P. Cunniffe, A. B. Preobrajenski, *J. Phys. Chem. C* **2014**, *118*, 12532–12540.

[13] K. A. Simonov, N. A. Vinogradov, A. S. Vinogradov, A. V. Generalov, E. M. Zagrebina, G. I. Svirskiy, A. A. Cafolla, T. Carpy, J. P. Cunniffe, T. Taketsugu, et al., *ACS Nano* **2015**, *9*, 8997–9011.

[14] M. Di Giovannantonio, M. Tomellini, J. Lipton-Duffin, G. Galeotti, M. Ebrahimi, A. Cossaro, A. Verdini, N. Kharche, V. Meunier, G. Vasseur, et al., *J. Am. Chem. Soc.* **2016**, *138*, 16696–16702.

[15] G. Galeotti, M. Di Giovannantonio, J. Lipton-Duffin, M. Ebrahimi, S. Tebi, A. Verdini, L. Floreano, Y. Fagot-Revurat, D. F. Perepichka, F. Rosei, et al., *Faraday Discuss.* **2017**, *204*, 453–469.

[16] K. A. Simonov, A. V. Generalov, A. S. Vinogradov, G. I. Svirskiy, A. A. Cafolla, C. McGuinness, T. Taketsugu, A. Lyalin, N. Mårtensson, A. B. Preobrajenski, *Sci. Rep.* **2018**, *8*, DOI 10.1038/s41598-018-21704-3.

[17] G. Galeotti, M. Di Giovannantonio, A. Cupo, S. Xing, J. Lipton-Duffin, M. Ebrahimi, G. Vasseur, B. Kierren, Y. Fagot-Revurat, D. Tristant, et al., *Nanoscale* **2019**, *11*, 7682–7689.

[18] M. Fritton, D. A. Duncan, P. S. Deimel, A. Rastgoo-Lahrood, F. Allegretti, J. V. Barth, W. M. Heckl, J. Björk, M. Lackinger, *J Am Chem Soc* **2019**, *141*, 4824–4832.

[19] W. Wang, X. Shi, S. Wang, M. A. Van Hove, N. Lin, *J. Am. Chem. Soc.* **2011**, *133*, 13264–13267.

[20] A. Basagni, F. Sedona, C. A. Pignedoli, M. Cattelan, L. Nicolas, M. Casarin, M. Sambi, *J. Am. Chem. Soc.* **2015**, *137*, 1802–1808.

[21] S. J. Blanksby, G. B. Ellison, *Acc. Chem. Res.* **2003**, *36*, 255–263.

[22] D. A. King, *Surf. Sci.* **1975**, *47*, 384–402.

[23] J. Björk, F. Hanke, S. Stafström, *J. Am. Chem. Soc.* **2013**, *135*, 5768–5775.

[24] M. Di Giovannantonio, G. Contini, *J. Phys. Condens. Matter* **2018**, *30*, 093001.

[25] J. F. Dienstmaier, A. M. Gigler, A. J. Goetz, P. Knochel, T. Bein, A. Lyapin, S. Reichlmaier, W. M. Heckl, M. Lackinger, *ACS Nano* **2011**, *5*, 9737–9745.

[26] C.-Z. Guan, D. Wang, L.-J. Wan, *Chem. Commun.* **2012**, *48*, 2943.

[27] X.-H. Liu, C.-Z. Guan, S.-Y. Ding, W. Wang, H.-J. Yan, D. Wang, L.-J. Wan, *J. Am. Chem. Soc.* **2013**, *135*, 10470–10474.

Graphical abstract:

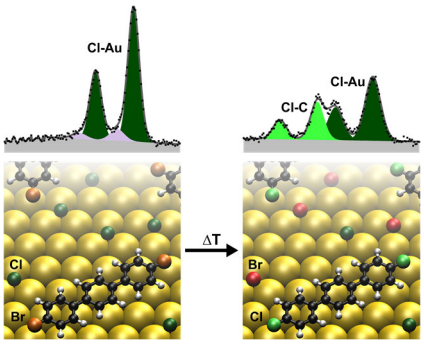

To reverse or not to reverse:

The initiating dehalogenation step in on-surface dehalogenative aryl-aryl coupling is evidenced to be reversible on Au(111), but not on Cu(111). This calls for a reassessment of reaction pathway and kinetics and discloses conditions to overcome current limitations in on-surface synthesis.